ROTOR STATE FEEDBACK IN ROTORCRAFT ATTITUDE CONTROL

Simone Panza
Marco Lovera
Dipartimento di Scienze e Tecnologie Aerospaziali, Politecnico di Milano, Italy

Marco Bergamasco
Luca Viganò
AgustaWestland, Cascina Costa, Italy

Abstract

An approach to rotor state feedback attitude control aimed at nominal stability, closed-loop performance, uncertainty robustness and tolerance to rotor state feedback faults is proposed. Structured H_∞ control based on a reduced linearized FlightLab model, an uncertainty description (changes in mass, altitude, center of mass position, speed) and requirements on the sensitivity functions is used to optimize tunings for given controller structures.

1. INTRODUCTION

Rotorcraft attitude control systems aim at providing a fast and accurate attitude response while rejecting external disturbances, such as wind gusts. As is well known, attitude control gains can be tuned so as to achieve a trade-off between disturbance rejection bandwidth [1,4] and damping of oscillations in the attitude response. This trade-off between disturbance rejection bandwidth and damping ratio has been studied extensively in recent years [5,6,10] as it is of fundamental importance to understand its mechanism to assess the achievable closed-loop performance levels.

Rotor state feedback [6,8,11,12,14] (RSF) has been studied by a number of authors as a means to overcome performance limitations inherent in conventional attitude control. Indeed, research on RSF has shown that the introduction of rotor state measurements in the feedback control law, in addition to inertial measurements, has the potential to overcome the trade-off between bandwidth and damping: higher disturbance rejection bandwidth can be achieved, while keeping sufficiently high levels of damping. The reason for this performance improvement lies in the coupling between attitude and rotor dynamics in the frequency range over which the attitude control loop is closed: thus, adding rotor state measurements to the feedback control law introduces information about rotor dynamics in the loop and leads in turn to better performance. The issue of rotor-fuselage coupling and its importance in the synthesis of high-bandwidth attitude control laws was extensively studied [7,9,14,15].

The aim of this paper (which builds on preliminary results presented in previous work from the authors [11,12]) is to propose a systematic approach to the design of structured RSF attitude control laws, with the following properties: nominal stability and prescribed performance of the closed-loop system; robustness to model uncertainty due to, *e.g.*, changes in the flight condition, configuration *etc.*; fault tolerance with respect to openings of the RSF feedback channel. The proposed methodology is based on the following steps. A nominal control-oriented design model is obtained by suitable model reduction of a reference linearized FlightLab model, augmented with dynamics for actuators and sensors; an output-multiplicative representation of uncertainty is then generated by taking into account variations of mass, altitude, center of mass position and forward speed. Design requirements originally provided in terms of settling time, damping, disturbance rejection bandwidth *etc.*, are encoded in terms of frequency-dependent weights on the closed-loop sensitivity functions (sensitivity, control sensitivity, complementary sensitivity) and a mixed-sensitivity H_∞ synthesis problem is formulated. The optimal solution to the problem is computed in a structured framework, *i.e.*, by seeking optimal values for the parameters of a predefined controller structure.

With respect to previous work [12], where the impact of RSF on the closed-loop performance was studied under the assumption of ideal rotor state measurements, in this paper a realistic model of the blade motion sensor is introduced, and the performance improvement achievable in realistic conditions is assessed, compared to the ideal measurements case.

Finally, the study of robustness with respect to

variations of model parameters (mass, altitude, center of mass position) performed in previous work [12] is further carried on, taking into account also variations of forward speed; *a posteriori* closed-loop analysis is performed, and it is shown that the regulator synthesized on the nominal model is robust to realistic parameters variations.
The results presented in this paper are part of an investigation of RSF in the framework of the CleanSky GRC5 MANOEUVRES project [16,17], the primary goal of which is the development of an innovative rotor sensor system capable to deliver real-time information on the rotor state and conceived in view of its application on production rotorcraft. In this framework, an effort towards innovation in rotorcraft control, aimed at control strategies enabled by the availability of novel sensors for in-flight rotor state measurement, is envisaged.

2. CONTROL-ORIENTED MODELING

A control-oriented model, namely a helicopter model which retains the dynamics of the vehicle in the frequency range interested by attitude control, was obtained. The hover case and the forward speed cases have been studied and compared to highlight similarities and differences between them. In this respect, it is important to keep into account the fuselage-rotor coupled dynamics during the modeling phase, since one of the objectives of this study is to assess the closed-loop characteristics of the system when a rotor state feedback control law is employed.

2.1 Hover case

For the purpose of this study, a sample linearized FlightLab model has been provided by AgustaWestland. The model, corresponding to 58 states, linearized in hover, takes into account both fuselage and rotor dynamics; in particular, body dynamics (Euler angles, angular rates, translational velocities), main rotor dynamics (flap and lag angles in Multi-Blade Coordinates (MBC) and their derivatives), main rotor inflow model (10 states), main rotor wake model (3 states) and tail rotor dynamics (collective inflow and coning angle) are modeled. The model takes into account the four classical helicopter control inputs: main rotor collective, lateral and longitudinal cyclic, and tail rotor collective.
Actuator and sensor dynamics have been cascaded upstream and downstream to the FlightLab model. Moreover, an equivalent time delay of 20 ms was cascaded to the model, in order to take into account delays related to signal processing and Zero-Order Holding (ZOH). A third-order Padé approximation of the pure time delay was used.

For the sake of attitude control law synthesis, the full-order augmented model was reduced. Details about the model reduction procedure can be found in a previous paper [12]; in short, the model reduction procedure consists of the following steps:

- a truncation procedure, aimed at dropping all those states which are not relevant to the lateral-longitudinal attitude control problem (*e.g.*, states related to translational speed, and states related to yaw and heave dynamics); this leads the 58 states model to 25 states;
- a modal decomposition-based approach, which, on the basis of the result of the previous step, has the aim to decompose the frequency response of interest into the sum of its modal components, in order to retain only the most significant ones in terms of magnitude.

Focus was put on the lateral axis; the result of the model reduction procedure is an approximate second order model of the (on-axis) lateral attitude dynamics. It turned out [11,12,14] that it is of fundamental importance to keep into account the coupling between fuselage and rotor; indeed, the lateral attitude dynamics is mostly influenced by the regressive flap mode, which is second order and is retained by the reduced order model. This justifies the need for a fully coupled model of the fuselage-rotor dynamics when a high bandwidth attitude control loop is taken into account [7,9,15].
Moreover, in order to take into account the phase delay due to neglected higher order rotor modes, and to actuator and sensor dynamics, a pure time delay has been introduced in the second order model.
In this way, a 3x1 model of the lateral attitude dynamics was obtained; the model takes as an input lateral cyclic, and gives back as outputs the measurements of roll rate p, roll angle φ (which is computed as the integral of p) and lateral flap β_{1s}; the model is second order, indeed the retained regressive flap mode dominates the frequency response of all the three transfer functions.

2.2 Forward speed case

The analysis so far summarized [12] is now further developed, with the aim of considering, in addition to the hover condition, also the forward speed condition: as in Section 2.1, two more models were obtained by linearization at different forward speed values, namely 50 kts and 90 kts, all the other parameters being equal (mass, altitude, center of mass position). As for the nominal model in hover, also models in forward speed are obtained by FlightLab and are 58 states linearized models.
This section is devoted to the analysis of the nominal models in forward speed, *i.e.*, to an analysis

of the open loop on-axis frequency responses, in order to highlight similarities and differences with respect to the hover nominal case. Then, the approach of model reduction based on modal decomposition, which was applied to the hover nominal model, is applied to the forward speed case. A comparison between the nominal model in hover and the 50, 90 kts models was carried out. Figure 1 shows the magnitude of the frequency response from lateral cyclic to roll rate; in the (normalised) frequency range [0.6-3] the magnitude is basically the same for the frequency responses at all the considered speeds. At low frequency the behaviour is significantly different, especially in the hover case, where a very lightly damped lateral oscillation mode at a frequency between 0.1 and 0.2 appears with a high resonance peak, and the DC gain is significantly lower with respect to the other two models; this different behaviour at low frequency does not represent a problem from the point of view of attitude control, which instead focuses on the medium frequency range. Differences at high frequency (>3), in correspondence of rotor dynamics are less significant.

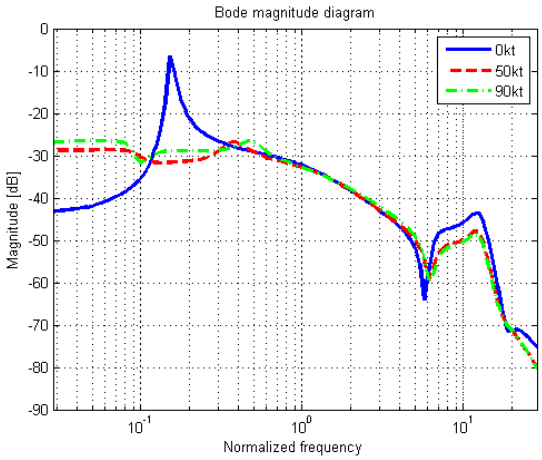

Figure 1 Nominal model, hover vs 50 vs 90 kts: magnitude of frequency response from lateral cyclic to roll rate.

The full order model was then reduced; again, in order to perform the model reduction, the modal decomposition approach has been chosen. As an example, Figure 2 shows the modal decomposition applied to the transfer function from lateral cyclic to roll rate of the 90 kts model; it is evident that the predominant component (in the figure, the line in black-squares related to the modal component with highest magnitude) is related to a pair of conjugate complex eigenvalues, which has been named “lateral attitude”. The pair of regressive flap poles (which are related to a modal component shown in black solid line in the figure) plays a less relevant role in the modal decomposition, but is still vital in approximating the lateral attitude dynamics, as it will turn out in the following. Finally, a low-frequency mode associated with translational dynamics and a higher frequency mode, associated with inflow dynamics, have been selected among the most influential modal components.

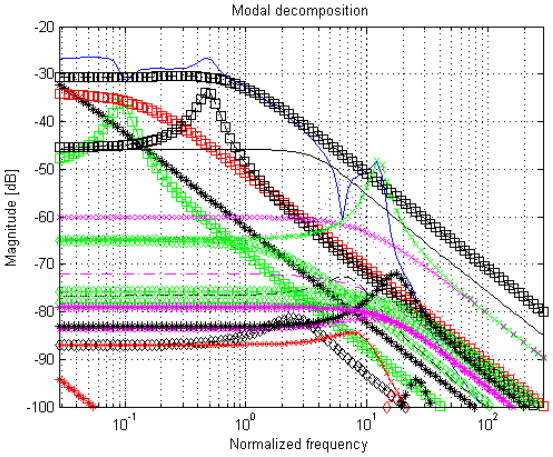

Figure 2 Modal decomposition, 90 kts case, transfer function from lateral cyclic to roll rate.

Based on such considerations, several reduced order models of increasing complexity were obtained with the modal decomposition approach; such models were then compared to the full order model to highlight advantages and drawbacks of each model, and finally a model was chosen to approximate the full order model in the attitude dynamics range of frequency, so as to achieve a reasonable trade-off between complexity and accuracy.

Figure 3, as an example, shows the comparison between the Bode diagram of three reduced order models (namely a model of order two, four and five, respectively) with respect to the full order model.

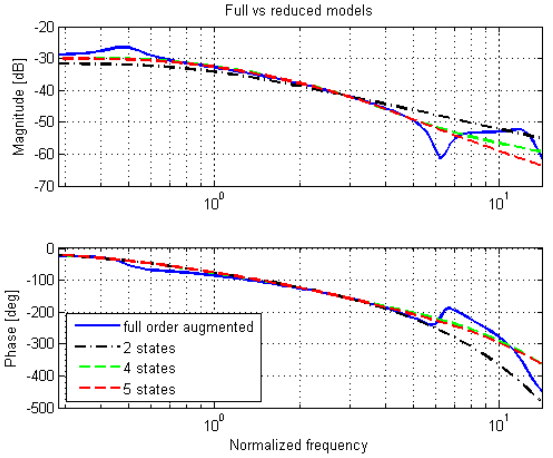

Figure 3 Comparison, 90 kts, lateral cyclic to roll rate, full vs reduced order models.

It is evident that the simplest model of order two (which contains only the two poles which have been referred to as “lateral attitude”) cannot approximate in a satisfactory way the magnitude plot of the frequency response of the full model, while the order four and five models can satisfactorily

approximate the magnitude, at least in the frequency range [0.3, 3], which is relevant for attitude dynamics. The phase plot, on the other hand, is similar for all the models and well approximates the phase of the full order model.
In a similar fashion as in the hover case, a reduced order model for the transfer function from lateral cyclic to lateral flap was obtained. The model reduction approach for lateral flap was again based on modal decomposition; since rotor dynamics are strongly coupled to fuselage dynamics, the reduced order model of lateral flap shall retain the same dynamics described by the reduced order model of roll rate, in addition to further dynamics, if necessary.
Figure 4 shows the Bode plots of the frequency response of the two models: one model of order four, which takes into account the two poles related to lateral attitude and the two regressive flap poles; the other one of order five which, in addition, takes into account a pole related to the inflow dynamics. It is evident that the order four model is inadequate to describe the full order model, both in the magnitude and in the phase; on the other hand, the model of order five achieves a good approximation in the range of frequency [1-6].

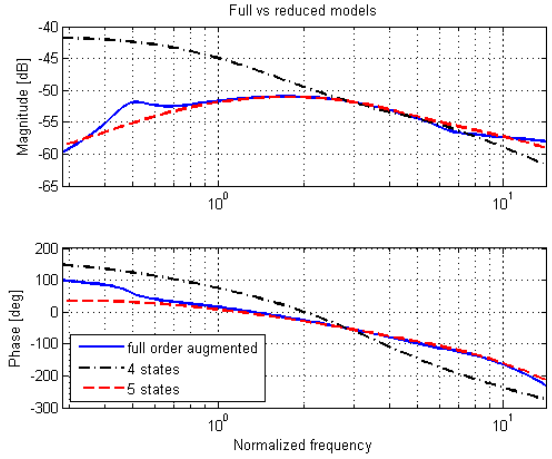

Figure 4 Comparison, 90 kts, lateral cyclic to lateral flap, full vs reduced order models.

Similarly, a reduced order model was obtained for the 50 kts case. Table 1 summarizes the order of the final choices for the reduced models, for different forward speeds, both for the transfer function from lateral cyclic to roll rate, and from lateral cyclic to lateral flap. The first difference between the hover and the forward speed case is about the order of the roll rate model:

- in the hover case a second order (related to two regressive flap poles) model was deemed sufficient to approximate the lateral attitude dynamics;
- in the forward speed case, in addition to the regressive flap dynamics, another second order dynamics (which has been referred to as “lateral attitude” poles) has to be taken into account, leading to a model of at least order four.

Moreover, if the lateral flap dynamics is taken into account too, the inflow dynamics plays a relevant role as well:

- in the 90 kts case, it is sufficient to introduce a first order mode related to inflow dynamics, hence the model becomes of order five;
- the 50 kts case seems to be more influenced by inflow dynamics, and a model of order ten was employed in order to accurately approximate the full order model.

The 50 kts condition seems to be critical in this respect - inflow dynamics play a relevant role in the dynamics of lateral flap.

Forward speed [kts]	Order (roll rate)	Order (lateral flap)
0	2	2
50	5	10
90	5	5

Table 1 Final choice of the order of reduced models; hover, 50 kts, 90 kts.

3. CLOSED-LOOP ANALYSIS

In this section the closed-loop behaviour of the helicopter will be studied. An ACAH (attitude command, attitude hold) command configuration will be taken into consideration in the following [1]. Focus will be put on the attitude control loop (inner loop), which is in charge of tracking the attitude commanded by pilot; this is the control loop which can benefit from the most relevant improvements deriving from RSF, and is closed at high frequency. The velocity (outer) loop, which is closed at lower frequency and is not influenced by RSF, is neglected. The attitude control loop is closed for each axis separately. No decoupling between axes is taken into account, for the time being. Most of the details have been omitted, and can be found in a previous paper [12].

3.1 Baseline attitude control law

The baseline control law is a PD controller on the attitude; as far as the roll axis is concerned, the required measurements are attitude angle φ and attitude rate p. The lateral cyclic control input δ_a is then computed as a linear combination of these measurements:

$$\delta_a = -\left(K_p p + K_\varphi \varphi\right).$$

The same holds true for the pitch axis, where the measurements are respectively θ, q and the control input is the longitudinal cyclic δ_e.
Figure 5 shows the closed-loop bandwidth and

damping ratio for different lateral axis control laws; the bandwidth is computed based on the sensitivity function (the closed-loop transfer function from output disturbance to φ), which is also referred to as the disturbance rejection bandwidth (DRB); the damping ratio is computed based on the closed-loop regressive flap poles location, since the regressive flap mode dominates the roll attitude dynamics.
The graph is meant to be read along two directions:

- each curve represents a different value of K_φ. Starting from the top-left corner of the figure, and proceeding towards the bottom-right corner, K_φ increases (from 50 to 290); the curves - which have a "hill" shape - move to the right, and their peak reduces. The shift to the right is due to the fact that, when K_φ increases, then also bandwidth increases; the peak reduction is related to a smaller damping; so, the trend is: the higher the bandwidth, the lower the damping;
- focusing on one curve at a time, each point of the curve represents a different $\frac{K_p}{K_\varphi}$ ratio value, *i.e.*,
  $\frac{K_p}{K_\varphi} = [0.02, 0.04, 0.06, 0.08, 0.1, 0.13, 0.2, 0.25, 0.3, 0.5, 1]$.
  Starting from the right end of the curve, and proceeding to the left, climbing the hill and descending, the ratio $\frac{K_p}{K_\varphi}$ increases, from 2% to 100%. Each curve reaches a peak, which is the maximum achievable damping ratio, having K_φ fixed.

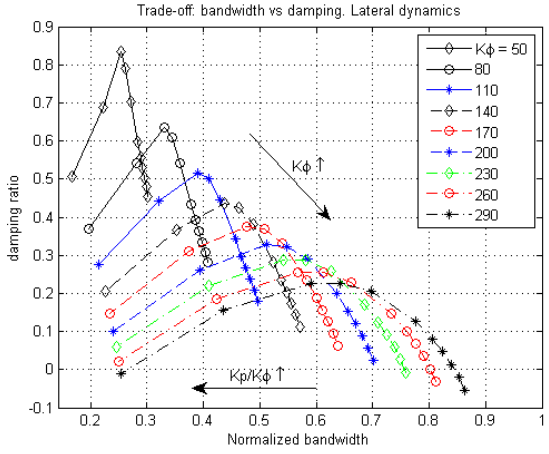

Figure 5 Baseline control law: trade-off between bandwidth and damping ratio, lateral axis.

As Figure 5 shows, there exists a performance limit, represented by the envelope of all the points: in other words, there is a trade-off between bandwidth and damping ratio, a maximum performance achievable by the baseline control law; the best combinations of bandwidth/damping ratio lie on the envelope of the graph, and that is the limit performance which can be obtained with a baseline control law. The bandwidth cannot be increased arbitrarily as at some point the damping would become too small to be tolerated; points that lie under the null damping ratio horizontal line represent unstable systems, and the rightmost point in the graph which is at the same time stable, lies at a (normalized) bandwidth of about 0.85.

3.2 RSF vs baseline performance

Up to now, only a baseline control law has been considered, which exploits fuselage measurements. Let now rotor state measurements be introduced. The MBC transformation is applied to flap and lag angles of rotor blades; in particular:

- the lateral axis is most influenced by lateral flap angle β_{1s} (which is related to the lateral thrust component, which in turn causes a roll moment) and by lateral lag angle ζ_{1c} (which can be interpreted as the rotor blades center of mass offset in the lateral direction, thus again related to a roll moment), so these two measurements are eligible to be introduced in the roll axis feedback control law;
- on the other hand, the longitudinal axis is most influenced by longitudinal flap β_{1c} and longitudinal lag ζ_{1s}, for reasons analogous as above.

In particular, as far as the roll attitude is concerned, a control law which exploits feedback measurement of lateral flap β_{1s} will be considered; the RSF control law is a static output feedback:

$$\delta_a = -\left(K_{\beta_{1s}}\beta_{1s} + K_p p + K_\varphi \varphi\right).$$

The introduction of lateral flap measurement in the control law has the effect of moving the regressive flap poles into regions of the complex plane where the damping ratio is much larger with respect to the baseline control law ($K_{\beta_{1s}} = 0$), up to a certain point beyond which the damping ratio no longer increases.
The same procedure undertaken when assessing the bandwidth-damping trade-off for the baseline case was repeated for the RSF case, for different values of $K_{\beta_{1s}}$.
In Figure 6, which is related to the roll axis, a cloud of red points shows a set of the possible control law configurations for the baseline case (which basically correspond to the same points of Figure 5, in which $K_{\beta_{1s}} = 0$), while blue points are referred to the RSF case (different combinations for the three gains $K_{\beta_{1s}}, K_p, K_\varphi$). The effect of introducing rotor state measurements in the control law is that the cloud of points expands in the top-right direction with respect to the baseline red cloud, and this enables to reach larger bandwidth at equal damping, or vice versa. RSF thus makes it possible to overcome the trade-off between bandwidth and damping which emerged

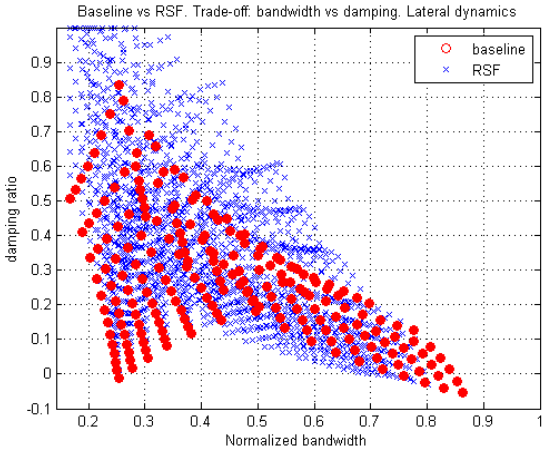

Figure 6 Baseline vs RSF: trade-off between bandwidth and damping ratio, lateral axis.

in the baseline control law.
It is important to remark that introducing RSF does not allow to raise the *maximum* reachable bandwidth (in fact, there are no blue points at the right end of the graph, beyond red points): the bandwidth is essentially determined by K_φ; however, at equal bandwidth, RSF allows to achieve a better damping ratio, that is, RSF makes it possible to cover regions in the complex plane that were not reachable in the baseline case, due to inadequate damping ratio. In this sense, RSF makes it possible to *increase the bandwidth*.

3.3 RSF performance: ideal vs real sensor

One of the main objectives of this study is to compare the benefits in terms of performance improvement attainable by RSF, assuming an ideal rotor state sensor is available, to the performance actually achievable in presence of a realistic rotor state sensor. In this perspective, the results obtained for the ideal measurements case [12] serve as a benchmark to be compared to the case of realistic measurements. The analysis previously performed [12] is here replicated, cascading the dynamics of the rotor flap sensor to the output of the open loop helicopter model; a numerical model of the sensor is provided as a result of the activity of flapping measurement system characterization performed in the framework of MANOEUVRES CleanSky project.
One of the main differences between the cases of ideal and realistic flap measurement consists in that, while the ideal measurement is a continuous time signal, in the actual measurement system the signal will be digital. Digitalization introduces both quantization and a time delay in the measurement: assuming the signal is sampled at a sampling frequency f_S of approximately 35 Hz (which corresponds to a sampling period $T_S = 1/f_S$), and that the rotor flap sensor could be characterized as a pure time delay, as a worst-case the effect of digitalization of the signal can be represented by a pure time delay equal to one sampling period $\tau = T_S$. Figure 7 shows the open loop response of transfer function from lateral cyclic to lateral flap, in the ideal case (without sensor) and in the realistic case (with sensor modeled as a time delay of one sample); the presence of the time delay has no effect on the magnitude of the frequency response, but it introduces phase lag in the system.

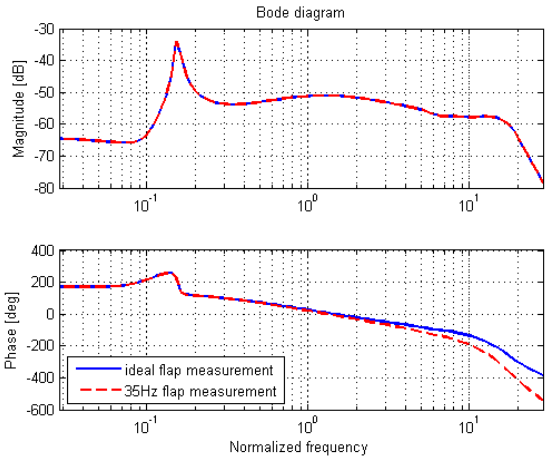

Figure 7 Frequency response, lateral cyclic pitch to lateral cyclic flap: ideal vs realistic flap measurement.

Figure 8 and Figure 9 show closed-loop responses to a step in roll angle reference; the case of ideal sensor ($\tau = 0$) is compared to the case of realistic sensor (f_S = 35 Hz), which corresponds to $\tau = 1/F_S \simeq 0.029$ s) and to an extreme case in which the sampling frequency is very low, namely 1 Hz. Time responses for the ideal and the 35 Hz cases are very similar, which suggests that the closed loop performance is not significantly affected by delay due to digitalization at such a sampling frequency.

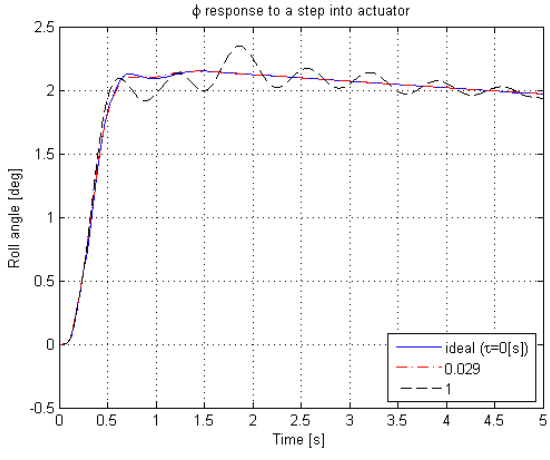

Figure 8 Closed loop step response: roll angle, ideal vs realistic flap measurement.

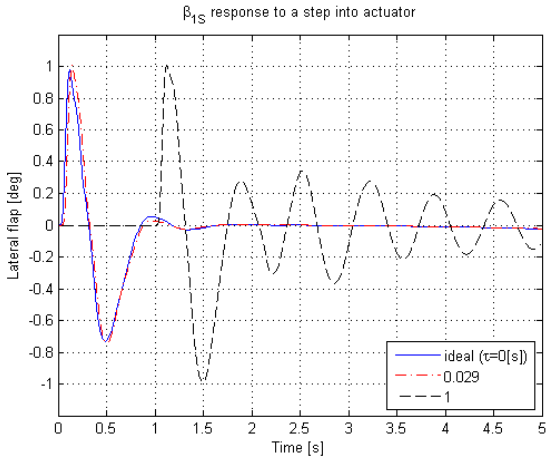

Figure 9 Closed loop step response: lateral flap, ideal vs realistic flap measurement.

It is interesting to notice, however, that in the extreme case of 1 Hz sampling, oscillations occur both in the roll angle and in the lateral flap responses, with tendency to reduce the damping ratio of such oscillations as the sampling frequency decreases; as a consequence, phase margin reduces, nevertheless the system is not driven to instability, even for lower values of sampling frequency.

4. MODEL UNCERTAINTY

In this section, the issue of model uncertainty with respect to physical parameters variations is addressed. The physical parameters which have been taken into account are mass, altitude, and center of mass offset in the three directions. A set of linearized model was provided by AgustaWestland, taking into account different combinations of these parameters (details are omitted for confidentiality reasons); one set of models was generated for each of the three speed points of 0, 50, 90 kts. Notice that the models used throughout this work up to now (obtained in Section 2) are linearized in the nominal parameter values and will be referred to as the nominal models. The nominal model in hover will be the basis on which the model uncertainty description will be defined. The other models in the set will be referred to as the "perturbed", or "off-nominal" models.

In the hover case, which was taken into account in the previous paper [12], an analysis of sensitivity to the parameter variations on the frequency responses on the main axes was performed; it was highlighted that the most relevant effects of mass, altitude, CoM offset variations show up at low frequency, on the translational dynamics; on the other hand, the lateral axis frequency response does not seem to be particularly influenced by these parameter variations, at least in the frequency range interested by fuselage attitude dynamics. In conclusion, since little variability is evidenced on the fuselage attitude dynamics, parameter variations are expected not to influence in a significant way the closed-loop robustness of the attitude loop.

A similar analysis carried out in the forward speed case showed that the same considerations hold true as far as the forward speed perturbed models are concerned.

As a subsequent step, a description of uncertainty of the set of off-nominal models with respect to the nominal one is obtained, in the form of multiplicative uncertainty; such uncertainty description may be then used either to perform *a posteriori* analysis of robustness of the closed loop system, or directly into the control law synthesis phase, thus ensuring the so-obtained control law guarantees closed loop robustness to uncertainty.

4.1 Perturbed models: open loop analysis

In order to assess how sensitive the model is to variations of the parameters values, frequency responses of the perturbed models have been plotted versus the response of the nominal model; focus was put on the lateral axis (transfer function from lateral cyclic to roll rate).

In the hover case, shown in Figure 10, the nominal model (in red) is plotted against the whole cloud of perturbed models (blue); intuitively, the wide gap between the minimum and maximum magnitude value in the cloud of models at low frequency (<0.3) suggests that uncertainty is significant in this range of frequency; however, at higher frequency (>0.3), the gap becomes narrower. On the same figure are plotted also the frequency responses of the 50 and 90 kts nominal models: in the range of frequencies [0.6-3] the nominal responses are encompassed into the cloud of perturbed models in hover.

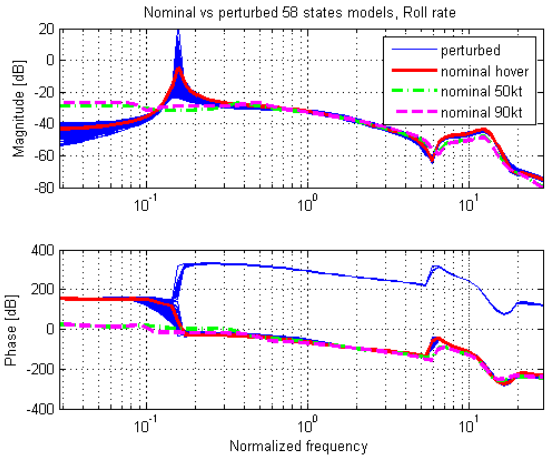

Figure 10 Nominal vs perturbed models: Bode plot of lateral axis frequency response (lateral cyclic to roll rate). Hover, 50 kts, 90 kts nominal models vs hover perturbed models.

Figure 11 shows a comparison between the frequency response of the nominal 90 kts model versus the cloud of perturbed models in the 90 kts case, showing that, even in the forward flight case, the parameter variations taken into account have a significant impact at low frequency, but not in the frequency range interested by attitude dynamics. Similar considerations hold true for the 50 kts case, here not shown for simplicity.

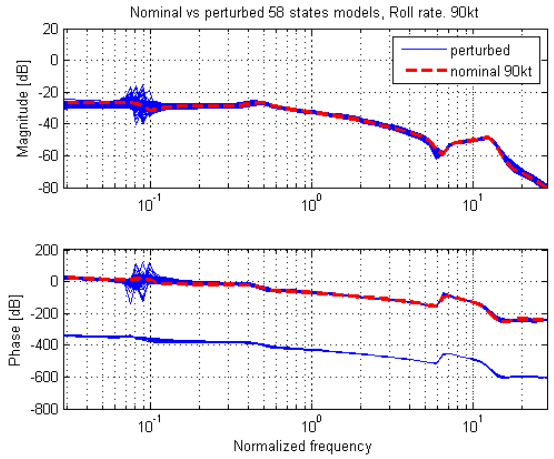

Figure 11 Nominal vs perturbed models: Bode plot of lateral axis frequency response (lateral cyclic to roll rate), 90 kts.

Two conclusions can be drawn from these considerations:

- If focus is put on the hover case, the small magnitude of uncertainty over the attitude dynamics frequency range suggests that the closed-loop system should not be significantly affected by robustness issues, in the case the regulator computed on the nominal model is closed on one of the perturbed models among those encompassed into the cloud.
- Extending the scope to the forward speed case, since the 50 kts and 90 kts nominal models are encompassed into the cloud as well, it is expected that the nominal regulator computed in the hover case shall not suffer from robustness issues even if it is used in the forward speed case, *i.e.*, the regulator is robust with respect to forward speed variations.

4.2 Uncertainty description

Once a nominal model and set of perturbed models have been obtained, it is necessary to formulate an uncertainty description in order to quantify the uncertainty of the set of perturbed models with respect to the nominal model. Indeed, the nominal model shall be used for the sake of control law synthesis, thus obtaining a nominal closed loop system which meets nominal stability and performance properties; the uncertainty description shall accomplish to the objectives of:

- assess *a posteriori* the robustness of the nominal closed loop system with respect to uncertainty (consistently with the amount of uncertainty introduced by the set of perturbed models).
- Perform robust control law synthesis, *i.e.*, to take into account the uncertainty description directly into the synthesis phase, so as to obtain a controller which guarantees robustness requirements are met.

One way to represent uncertainty as a function of frequency is by means of multiplicative uncertainty, as shown in Figure 12: the basic idea is to cascade to the nominal system $G(s)$ the parallel of two branches, namely a direct (nominal) branch, and another branch related to uncertainty, where $W_O(s)$ is a stable transfer function and represents a frequency weight, while $\Delta_O(s)$ is a stable, uncertain transfer function, bounded in magnitude. In this framework, $W_O(s)$ establishes the amount of uncertainty as a function of frequency; the higher the uncertainty, the largest the magnitude of $W_O(s)$.

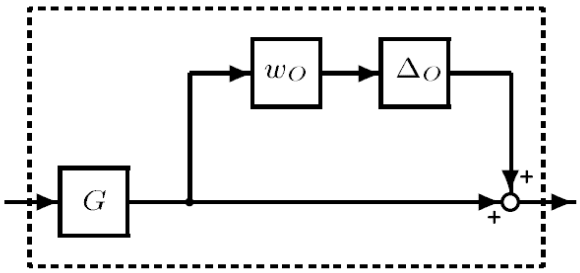

Figure 12 Multiplicative uncertainty description.

In the SISO case, the multiplicative uncertainty representation can be obtained by the set of perturbed models by computing for each of the perturbed models the corresponding multiplicative uncertainty: let $\bar{G}(s)$ be the nominal model, then

$$G_{\Delta M,i} = \frac{G_i(s) - \bar{G}(s)}{\bar{G}(s)}$$

is the multiplicative uncertainty computed on the i_{th} model in the perturbed set; $W_O(s)$ can be taken as the envelope of all the individual uncertainty descriptions, as the worst case. The approach can be extended to the more general MIMO case [13].
As an example, the roll rate frequency response was considered; a multiplicative uncertainty description was computed, as shown in Figure 13, considering the set of perturbed models in hover; uncertainty description was computed both for the 58 and 25 states model (see Section 2.1 for details about model reduction aspects). While the two of them are very similar at high frequency (>0.6), the same does not hold true at low frequency; in particular, as far as

the 58 states model is concerned, there is a significant amount of uncertainty below a frequency of 0.01 (almost 0 dB), and a very remarkable peak of uncertainty in the neighborhood of the lateral oscillation mode. This is due to the fact the 58 states model takes into account low frequency dynamics related to translational modes, which are very sensitive to parameter variations, and which are neglected by the 25 states model. However, uncertainty seems to be of small entity in the [0.3, 3] frequency range, which is the one interested by the attitude dynamics (as confirmed by the analysis in the previous section): this suggests uncertainty should not be a concern in the control law synthesis.

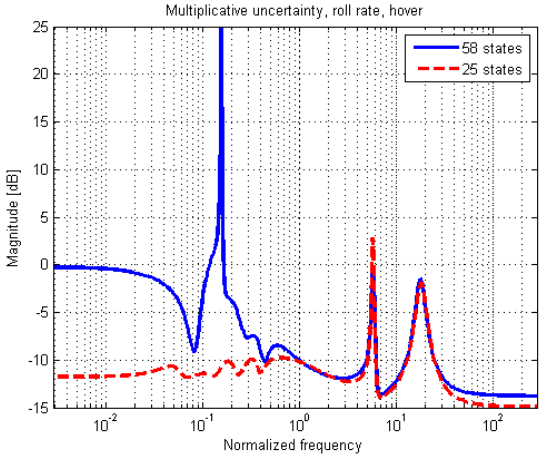

Figure 13 Multiplicative uncertainty on roll rate channel, hover case, 58 vs 25 states model.

In a similar fashion as in the hover case, the analysis was pushed further to the forward speed case and a multiplicative uncertainty description was obtained considering the whole set of perturbed models (hover, 50 kts, 90 kts); the so-obtained uncertainty description shall intuitively be more conservative than the one obtained in the hover-only case, since the set of perturbed models is larger.

As an example, multiplicative uncertainty on the roll rate channel is shown. Figure 14 shows, in blue, the multiplicative uncertainty computed for each of the perturbed models in hover, relative to the nominal model in hover; the black curve corresponds to the multiplicative uncertainty description if only models in hover are taken into account, *i.e.*, it corresponds to the blue curve shown in Figure 13. If the perturbed models in forward speed are introduced in the procedure of computation of the multiplicative uncertainty (here the multiplicative uncertainty cloud computed for the forward speed models is not shown for clarity), then the red curve is obtained. A weight of order 10 was employed to compute the uncertainty description; the red curve fits the upper bound of the set of curves in the frequency range [0.3-30], in order to avoid numerical issues at low frequency; this implies the uncertainty description is not accurate below a frequency of 0.3, in fact it can be seen that the red curve in Figure 14 cannot catch the peak of uncertainty at a frequency of about 0.2. The red curve lies over the old black curve, showing that by augmenting the set of perturbed models with the forward speed models, a more conservative uncertainty description is obtained; this shows up as an increased magnitude of the multiplicative uncertainty at a frequency of about 6. The increased level of uncertainty suggests higher sensitivity to robustness issues in closed loop; however, uncertainty in the frequency range [0.3, 3] remains on comparable levels as in the hover-only case.

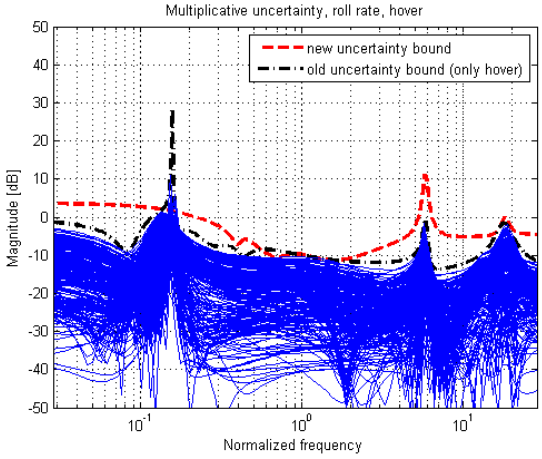

Figure 14 Multiplicative uncertainty on roll rate channel. Comparison between uncertainty description obtained in the hover-only case and hover+forward speed set of perturbed models. Blue curves correspond to the only hover case.

5. INNER-LOOP CONTROL LAW SYNTHESIS

Once the structure of the control law has been chosen (*e.g.*, as a static output feedback as seen in Section 3) and the control requirements have been defined, a control law synthesis approach is needed, such that the closed loop system achieves the control requirements. Such a synthesis approach shall provide some means to formulate the control requirements, and must be able to tune the control law parameters, given an arbitrary control law architecture. Following the methodology proposed in a previous paper [11], the structured H_∞ approach was chosen.

Not unlike the classical H_∞ approach, in the structured H_∞ case the plant model is augmented with performance inputs and outputs, which are defined as signals that need in some sense to be minimized; an optimal regulator is computed such that the H_∞ norm of the system closed in loop with the regulator, from the performance inputs to the performance outputs, is minimized [13]. In this framework, performance inputs and outputs can be chosen such that the norm to be minimized is a function of the closed-loop sensitivity functions

(sensitivity, control sensitivity, complementary sensitivity), weighted with proper frequency weights; control requirements are thus encoded as the frequency weights.

In the classical H_∞ approach the optimization problem is solved without constraints on the structure and order of the controller, which implies that the obtained regulator is of high order (the sum of the order of the plant and of the frequency weights) and it is a full matrix from all the measurable outputs to all the control inputs of the plant; in the case of rotorcraft flight control systems, both these issues represent a limitation to the feasibility of the classical H_∞ approach, since the control law architecture is often fixed and simple, and the computational power on board is limited.

The structured H_∞ approach, on the other hand, can cope with both these issues and overcome the limitations of the classical H_∞ approach: the main difference with respect to the latter is that the structure of the control law can be defined *a priori*; the optimization algorithm tunes the parameters of the control law such that the H_∞ norm is minimized. This requires non-smooth optimization techniques to be employed [3]; such techniques allow new constraints to be added to the optimization process, which would not be available by means of classical H_∞, hence control requirements of different nature can be introduced in the control synthesis problem [2]. It should be remarked that by means of structured H_∞, the methodology presented herein can be applied to already existing flight control law structures, provided that the control law parameters are not fixed a priori and can be tuned. On the other hand, of course the so-obtained solution is sub-optimal with respect to the solution of the classical H_∞ problem, since the number of degrees of freedom is significantly lower. The control law synthesis methodology presented in a previous paper [11] was applied to reduced order models here obtained; control requirements were formulated as follows:

- performance requirements were formulated as a weight on the attitude sensitivity function (on the φ channel);
- control moderation requirements were formulated as a weight matrix on the control sensitivity function: these requirements can also be interpreted from the point of view of measurement noise rejection requirements;
- the requirement of robustness with respect to uncertainty is formulated as a multiplicative uncertainty description and is a weight on the complementary sensitivity function.

To highlight the benefits of RSF with respect to a baseline control law, two sets of performance requirements for the feedback system have been defined: a set of *soft* requirements, with low bandwidth; a set of *hard* requirements, with higher bandwidth; the parameters of the weighting functions on roll sensitivity are shown in Table 2.

	soft	*hard*
Desired bandwidth (normalized)	0.43	0.57
DC gain K_{DC}	500	500
High frequency gain K_{HF}	0.9	0.5

Table 2 Performance requirements formulated as weight on the roll attitude sensitivity function.

Similarly, two sets of requirements concerning the rejection of measurement noise have been defined: a *soft* and a *hard* set of requirements, the latter emphasizing improved performance in terms of high frequency noise attenuation.

In selecting the control sensitivity weight, the high frequency pole was chosen keeping into account the actuators' bandwidth, assuming a (normalized) value of 14, in order to reduce out-of-bandwidth control action. Again, parameters for the weights on the roll control sensitivity functions are shown in Table 3.

	soft	*hard*
High frequency gain K_{HF}	$3.5\text{x}10^{-3}$	$12\text{x}10^{-3}$
Pole frequency (normalized)	14	14
Ratio K_{HF}/K_{DC}	$5\text{x}10^{5}$	$5\text{x}10^{5}$

Table 3 Control action moderation requirements formulated as weight on roll control sensitivity function.

As far as the requirement of robustness to uncertainty is concerned, since the results of the uncertainty analysis shown in Section 4 evidence that uncertainty is negligible in the frequency range interested by attitude dynamics, it was deemed sufficient to perform just a robustness analysis *a posteriori* on the perturbed models closed in loop with the regulator computed on the nominal model.

Following the methodology proposed [11,12], in order to show the benefits of RSF over a traditional attitude control law, four different laws were designed with the H_∞ approach: a *baseline* (B) law, a *RSF hard* (RSF_H) law, a *soft* (RSF_S) law, and a *fault robust* (RSF_{FR}) law. In particular, the fault robust control law has been designed so as to obtain performance requirements similar to RSF_H in the nominal case, *i.e.*, in case the β_{1S} measurement is available, while it should achieve less demanding performance similar to the baseline law in case of a rotor sensor fault. In case of fault of the lateral flap sensor, in which case the β_{1S} measurement is simply put to zero.

	$K_{\beta_{1s}} \frac{[\%]}{[rad]}$	$K_p \frac{[\%]}{[rad/s]}$	$K_\varphi \frac{[\%]}{[rad]}$
RSF_H	88	76	259
RSF_S	12	45	91
RSF_{FR}	231	63	158
B	0	65	119

Table 4 Comparison between controllers for the four control laws obtained using the H_∞ approach, lateral axis. Hover case. Gains computed based on the 25 states model in hover.

Table 4 shows the values of the four control law gains for the lateral axis, tuned by H_∞ optimization (based on the 25 states model in hover). Table 5 shows gain values obtained applying the control law synthesis methodology to the reduced order models in hover, 50 kts and 90 kts obtained in Section 2; for each of the models, the same requirements both in terms of performance and control action moderation were imposed. A comparison between the gains obtained based on the two different models for the hover case shows that the numerical values of the gains are reasonably similar.

Forward speed	Name	$K_{\beta_{1s}} \frac{[\%]}{[rad]}$	$K_p \frac{[\%]}{[rad/s]}$	$K_\varphi \frac{[\%]}{[rad]}$
0 (hover)	B	0.00	73.28	128.90
	RSF_H	87.15	83.58	269.50
	RSF_S	8.43	47.29	92.83
50	B	0.00	63.67	125.28
	RSF_H	82.58	80.69	276.49
	RSF_S	2.25	42.84	96.35
90	B	0.00	60.16	122.38
	RSF_H	80.95	75.66	277.32
	RSF_S	-1.10	42.13	96.88

Table 5 Comparison between controllers for the four control laws obtained using the H_∞ approach, lateral axis. Hover + forward speed case. Gains computed based on the reduced order models.

6. ROBUSTNESS ANALYSIS

The multiplicative uncertainty description obtained in the previous section can be employed:

- to perform *a posteriori* analysis on the closed loop system and verify that the regulator computed on the nominal model achieves acceptable performance and stability even in the case the loop is closed on the perturbed models;
- during the control law synthesis phase, so as to obtain a robust control law.

An *a posteriori* robustness analysis on the closed-loop system, based on the control law gains obtained with the H_∞ approach and shown in Section 5, has been performed. Notice that these control laws were synthesized based on the nominal models, without taking into account the uncertainty description obtained in Section 4.2.

As far as closed loop robustness is concerned, two kind of *a posteriori* analysis can be performed: in the frequency domain, or in the time domain. Both kinds of analysis were performed based on the full order models.

Frequency domain analysis is based on the condition of robust stability with respect to multiplicative uncertainty, which can be formulated as a condition on the weighted complementary sensitivity [13]. In the general MIMO case, the condition of robust stability is formulated in terms of infinity norm of the complementary sensitivity function $T(s)$ weighted with the transfer matrix $W_T(s)$ as follows:

$$\|W_T(s)T(s)\|_\infty \leq 1 \Leftrightarrow \max_\omega \bar{\sigma}\big(W_T(\jmath\omega)T(\jmath\omega)\big) \leq 1,$$

Where by $\bar{\sigma}$ the maximum singular value of a frequency response function is denoted; the largest singular value represents an indication of the maximum magnitude the frequency response of the MIMO transfer matrix can reach, as a function of frequency.

In the SISO case, it is more intuitive to resort to the following definition of infinity norm:

$$\sup_\omega |W_T(\jmath\omega)T(\jmath\omega)| \leq 1.$$

The complementary sensitivity function $T(s)$ is obtained by closing the loop on the nominal model with the nominal regulator, based on the model outputs β_{1s}, p, φ, and is a [3x3] transfer matrix; it can be interpreted as the closed-loop transfer matrix from set-points on these variables to the outputs.

The weight $W_T(s)$ on the complementary sensitivity function represents the amount of multiplicative uncertainty with respect to the nominal model, as a function of frequency; $W_T(s)$ was chosen as a square diagonal matrix of the same dimension as the model output, and each of the diagonal elements was chosen as the multiplicative uncertainty description obtained in Section 4.2 in the SISO sense, for the corresponding output.

The complementary sensitivity function was computed for the nominal model closed in loop with the B, RSF_H, RSF_S control laws, and then weighted with the multiplicative uncertainty description, in order to show possible closed-loop robustness issues. Two uncertainty descriptions were taken into account: the multiplicative uncertainty computed on the set of perturbed models in hover (hover-only case) and on the full set of perturbed models (hover+forward speed); the singular value plots of the weighted complementary sensitivity are shown respectively in Figure 15 and Figure 16. In particular, complementary sensitivity used in Figure 15 was computed based on the hover 58 states nominal model, closed in loop with the gain values shown in Table 4; on the other hand, the complementary sensitivity function used in Figure 16 was computed based on the 58 states model in hover, closed in loop with the gain values shown in Table 5 (hover).

Focusing on the "hover only" case (Figure 15), it is evident that the singular values of the baseline (B) and RSF soft (RSF_S) control laws always remain below the 0 dB threshold, thus indicating the robustness requirement is accomplished. The RSF hard law (RSF_H) exceeds the 0 dB bound in the [1-3] range of frequencies, although the peak is low (3 dB); this indicates the RSF_H control law anyway has good robustness properties.
On the other hand, if the amount of uncertainty is increased taking into account the "hover+forward speed" case (Figure 16), the situation is not significantly different. In this case, it must be remarked that the uncertainty description is accurate in the frequency range [0.3-30]. In the baseline and the RSF soft case, the singular values are always under the 0 dB line, thus the robust stability of the nominal regulator is guaranteed even in presence of uncertainty; the only case in which the largest singular value trespasses the 0 dB line, for some values of ω, is again the RSF hard case. Despite the increased amount of uncertainty (due to considering a larger set of perturbed models which encompasses also the forward speed case), the height of the peak of largest singular value is not significantly larger than the "hover only" case, thus suggesting that the regulators computed based on the nominal model shall not suffer from robustness issues. Moreover, this analysis suggests that there is not strict need to introduce the uncertainty description into the control law synthesis process (namely, to perform robust control law synthesis), although the control law synthesis methodology formulated so far would allow for it.

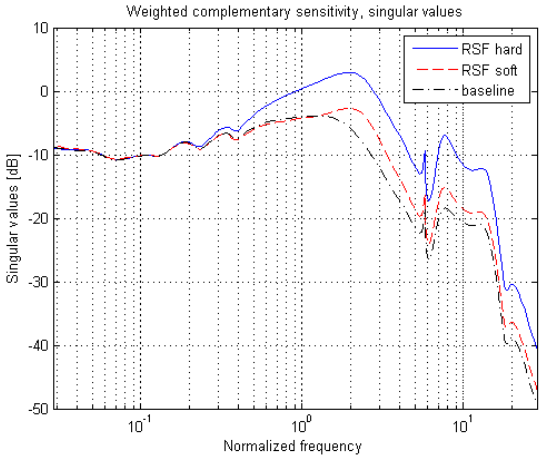

Figure 15 Weighted complementary sensitivity. Uncertainty description based on the set of perturbed models in hover ("only hover").

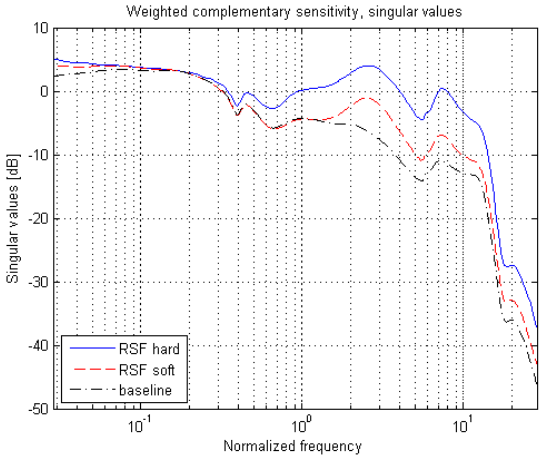

Figure 16 Weighted complementary sensitivity. Uncertainty description based on the full set of perturbed models (hover+forward speed).

Since the RSF hard law fails the robust stability test shown in Figure 16, focus was put on this control law, and *a posteriori* tests on the closed-loop system in the time domain were performed.
Figure 17 shows a set of responses of roll angle to a step reference; both the nominal model (in hover) and a representative set of perturbed models, at all speeds, was taken into account. The regulator is RSF_H (Table 5, hover). It is evident from the figure that the response of the perturbed models is very close to that of the nominal model, at least up to 1.5 s; the attitude dynamics dominates in this time window, and uncertainty in the attitude dynamics range of frequency has been proven to be of little relevance. There is some more relevant discrepancy between the responses in the time window [0.5-1.2] s, probably due to mass variations between the perturbed models, but the overall shape of the time response is the same for all the models.

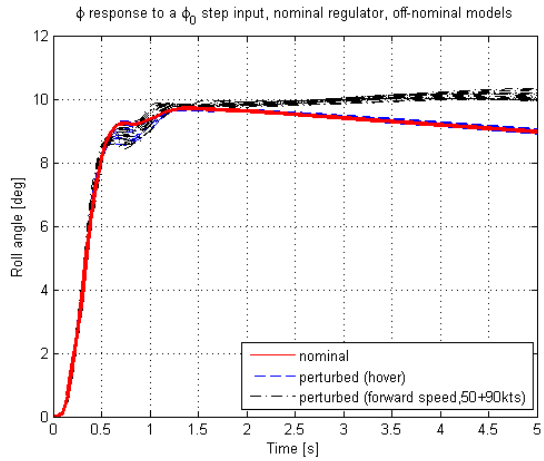

Figure 17 Closed loop step responses, RSF hard law. Roll angle response of nominal and perturbed models.

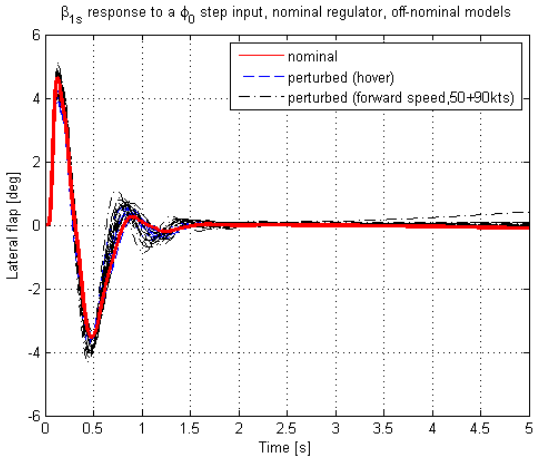

Figure 18 Closed loop step responses, RSF hard law. Lateral flap response of nominal and perturbed models.

After this threshold, low frequency dynamics come into play, and the behaviour of models at different speeds becomes very different; this can be explained, on the other hand, by the fact that uncertainty at low frequency is much more relevant with respect to the uncertainty in the attitude dynamics range of frequency.

Figure 18 shows the response of the lateral flap to a roll angle step reference, for the same set of models, with the RSF_H law; again, the time responses for the perturbed models are similar, and in particular the maximum excursion of lateral flap from the equilibrium value does not experience significant variations with respect to the nominal case.

In conclusion, not only stability is retained, but also performance seems to be close to the nominal one even when the regulator is closed on perturbed models.

7. CONCLUSIONS

The problem of rotorcraft attitude control has been studied, taking into account in the feedback control law traditional measurements related to fuselage (*i.e.,* attitude angles and angular rates) as well as measurements related to rotor state (*i.e.,* MBC flap angles). Rotor state feedback is potentially capable to improve the closed loop performance of the vehicle, in terms of disturbance rejection bandwidth and damping of oscillations, overcoming the trade-off between bandwidth and damping ratio which is intrinsic of a traditional control law.

Modeling aspects were taken into account as well; in particular, the coupling between fuselage attitude dynamics and rotor dynamics plays a fundamental role in defining the dominant closed loop dynamics when high bandwidth attitude control loop has to be closed; thus, an accurate fuselage-rotor coupled model of the vehicle is needed in the frequency range interested by attitude control. In particular, as far as lateral axis is concerned, the regressive flap mode is of fundamental importance in this coupling at all speeds; in the hover condition, a second order model which takes into account regressive flap can approximate the full-order model in a satisfactory way, while in the forward speed case higher order models are needed.

Tools to study closed loop robustness with respect to uncertainty have been presented. In particular, an uncertainty description in the multiplicative form has been used to quantify the uncertainty of a set of perturbed models with respect to a nominal model; such uncertainty description can be used either to perform *a posteriori* analysis on the closed loop system to verify robustness of stability, or directly into the control synthesis phase so as to obtain a robust control law. In the case considered, the control law was deemed to be sufficiently robust by means of *a posteriori* analysis, thus robust synthesis was not taken into account. For the time being, only the robustness properties of the on-axis channels are taken into account, while no solution has been devised for the off-axis channels (related to inter-axis coupling) yet.

Finally, an optimization-based methodology was defined, based on the modern structured H_∞ approach, which retains the benefits of the classical H_∞ approach and at the same time lets the control designer choose the control system architecture, thus being a feasible approach to helicopter control law synthesis. Control requirements from both standard specifications and from the literature were stated; a formulation of the H_∞ control problem based on weighted sensitivity functions optimization was proposed, and requirements were encoded into proper weighting functions.

ACKNOWLEDGMENTS

This research was partially supported by the CleanSky GRC5 MANOEUVRES project, grant agreement no. 620068.

REFERENCES

[1] ADS-33E-PRF, Aeronautical Design Standard, Performance Specification. Handling Qualities Requirements for Military Rotorcraft, March 2000.

[2] P. Apkarian. Tuning controllers against multiple design requirements. In *American Control Conference*, Washington DC, USA, 2013.

[3] P. Apkarian and D. Noll. Nonsmooth H_∞ synthesis. *IEEE Transactions on Automatic Control*, 51(1):71–86, 2006.

[4] C. L. Blanken, R. H. Hoh, D. G. Mitchell, and D. L. Key. Test guide for ADS-33E-PRF. Technical Report AMR-AF-08-07, AMRDEC, 2008.

[5] C. L. Blanken, J. A. Lusardi, C. M. Ivler, M. B. Tischler, M. T. Hofinger, W. A. Decker, C. A. Malpica, T. Berger, and G. E. Tucker. An

investigation of rotorcraft stability-phase margin requirements in hover. In *65th Annual Forum of the American Helicopter Society,* Grapevine, USA, 2009.
[6] J. F. Horn, W. Guo, and G. T. Ozdemir. Use of rotor state feedback to improve closed-loop stability and handling qualities. *Journal of the American Helicopter Society*, 57(2):1–10, 2012.
[7] S. J. Ingle and R. Celi. Effects of higher order dynamics on helicopter flight control law design. *Journal of the American Helicopter Society*, 39(3):12–23, 1994.
[8] C. M. Ivler. Development and comparison of explicit and implicit rotor-state feedback control systems for a fly-by-wire UH-60. In *AHS Rotorcraft Handling Qualities Specialists Meeting,* Huntsville, USA, 2014.
[9] W. E. Hall Jr. and A. E. Bryson Jr. Inclusion of rotor dynamics in controller design for helicopters. *Journal of Aircraft*, 10(4):200–206, 1973.
[10] M. H. Mansur, J. A. Lusardi, M. B. Tischler, and T. Berger. Achieving the best compromise between stability margins and disturbance rejection performance. In *65th Annual Forum of the American Helicopter Society,* Grapevine, USA, 2009.
[11] S. Panza and M. Lovera. Rotor state feedback in helicopter flight control: robustness and fault tolerance. In *IEEE Multi-Conference on Systems and Control,* Antibes-Nice, France, 2014.
[12] S. Panza and M. Lovera. Rotor state feedback in the design of rotorcraft attitude control laws. In *3rd CEAS Specialist Conference on Guidance, Navigation and Control,* Toulouse, France, 2015.
[13] S. Skogestad and I. Postlethwaite, Multivariable feedback control: analysis and design. J. Wiley and Sons, 1996.
[14] M. D. Takahashi. Rotor-state feedback in the design of flight control laws for a hovering helicopter. *Journal of the American Helicopter Society*, 39(1):50–62, 1994.
[15] M. B. Tischler. System identification requirements for high-bandwidth rotorcraft flight control system design. In *1991 American Control Conference,* Boston, USA, 1991.
[16] L. Trainelli, A. Rolando, E. Zappa, S. Manzoni, M. Lovera, M. Gennaretti, G. Bernardini, P. Cordisco, M. Terraneo, E. Vigoni, and R. Grassetti. MANOEUVRES - an effort towards quieter, reliable rotorcraft terminal procedures. In *Greener Aviation: Clean Sky Breakthroughs and worldwide status*, Brussels, Belgium, 2014.
[17] L. Trainelli, E. Zappa, A. Rolando, M. Lovera, M. Gennaretti, P. Cordisco, R. Grassetti, and M. Redaelli. Project MANOEUVRES - towards real-time noise monitoring and enhanced rotorcraft handling based on rotor state measurements. In *41st European Rotorcraft Forum ERF 2015 (accepted)*, Munich, Germany, 2015.